

This discussion paper is/has been under review for the journal Geoscientific Instrumentation, Methods and Data Systems (GI). Please refer to the corresponding final paper in GI if available.

# In-flight calibration of Hot Ion Analyser onboard Cluster

A. Blagau<sup>1</sup>, I. Dandouras<sup>2,3</sup>, A. Barthe<sup>2,3,4</sup>, S. Brunato<sup>2,3,5</sup>, G. Facskó<sup>6,7,\*</sup>, and V. Constantinescu<sup>1</sup>

<sup>1</sup>Institute for Space Sciences, Bucharest, Romania

<sup>2</sup>Institut de Recherche en Astrophysique et Planétologie, Université de Toulouse, Toulouse, France

<sup>3</sup>CNRS, Institut de Recherche en Astrophysique et Planétologie, Toulouse, France

<sup>4</sup>AKKA Technologies, Toulouse, France

<sup>5</sup>Noveltis, Toulouse, France

<sup>6</sup>Laboratoire de Physique et Chimie de l'Environnement et de l'Espace, Orléans, France

<sup>7</sup>Geodetic and Geophysical Institute, Research Centre for Astronomy and Earth Sciences, HAS, Sopron, Hungary

\*now at: Finnish Meteorological Institute, Helsinki, Finland

Received: 23 March 2013 – Accepted: 4 July 2013 – Published: 26 July 2013

Correspondence to: A. Blagau (blagau@spacescience.ro)

Published by Copernicus Publications on behalf of the European Geosciences Union.

## HIA in-flight calibration

A. Blagau et al.

Title Page

Abstract

Introduction

Conclusions

References

Tables

Figures

◀

▶

◀

▶

Back

Close

Full Screen / Esc

Printer-friendly Version

Interactive Discussion



## Abstract

The Hot Ion Analyser (HIA), part of the Cluster Ion Spectrometry experiment, has the objective to measure the three-dimensional velocity distributions of ions. Due to a variety of factors (exposure to radiation, detector fatigue and aging, changes in the operating parameters etc.), the particles detection efficiency changes over time, prompting for continuous in-flight calibration. This is achieved by comparing the HIA data with the data provided by the WHISPER experiment on magnetosheath intervals, for the high sensitivity section of the instrument, or solar wind intervals, for the low sensitivity section. The paper presents in detail the in-flight calibration methodology, reports on the work carried out for calibrating HIA and discusses plans to extend this activity in order to ensure the instrument highest data accuracy.

## 1 Introduction

The Hot Ion Analyser (HIA) and the COmposition and DIstribution Function (CODIF) analyzer are the two sensors of the Cluster Ion Spectrometry (CIS) experiment (Rème et al., 2001) onboard Cluster, having the objective to measure the three-dimensional velocity distributions of ions. As a major difference from CODIF, the HIA instrument does not provide mass resolution; however, HIA offers other important advantages, like higher detection efficiency, better angular and energy resolution, faster electronics capable to handle higher count rates etc.

HIA detection system is based on micro-channel plate (MCP) technology. The instrument efficiency has been determined on ground through extensive pre-flight calibrations. However, due to various reasons, like MCP gain fatigue and aging (Prince and Cross, 1971) or because of the penetrating radiation (in the radiation belts or from cosmic ray bombardment), the detector efficiency changes in the course of the mission, requiring periodic in-flight calibration. An in-flight calibration is needed as well whenever the HIA operating point is changed by commands from ground. The multi-point

GID

3, 407–435, 2013

## HIA in-flight calibration

A. Blagau et al.

Title Page

Abstract

Introduction

Conclusions

References

Tables

Figures

◀

▶

◀

▶

Back

Close

Full Screen / Esc

Printer-friendly Version

Interactive Discussion



character of Cluster and its complex payload made possible to assess the HIA in-flight performance at an unprecedented level of accuracy.

The calibration methodology to be presented in this paper was developed by taking advantage of the large cross-calibration effort carried on in the framework of ESA's Cluster Active Archive (CAA) program. Before the CAA initiative, the resources allocated to this activity were relatively small when compared with the complexity of the work; also, the less accurate Cluster Prime Parameter data set has been used as a reference for the total electron density (Vallat, 2001).

The CIS experiment is prepared by an international consortium, under the principal responsibility of Institut de Recherche en Astrophysique et Planétologie (IRAP) in Toulouse (formerly Centre d'Etude Spatiale des Rayonnements). Since 2009, the Institute for Space Sciences in Bucharest assumed a key role in HIA in-flight calibration, in close collaboration with IRAP.

The CIS data sets available through the CAA interface are described in Dandouras et al. (2010). An updated report on the CIS calibration activities can be found on the CAA web page (current version: 1.3, see Dandouras et al., 2012).

The paper is organized as follows: in Sect. 2 the instrument and its specific parameters are presented. Section 3 discusses the HIA operation modes and data caveats. Section 4 provides details on the calibration tasks and illustrates the calibration methodology by two examples. The next section presents two statistical studies carried out for validating the HIA in-flight calibration. In Sect. 6 the results of HIA in-flight calibration are summarized and plans to extend this activity are discussed.

## 2 Instrument presentation

Figure 1 presents the HIA operational principles. The instrument employs a 360° angle imaging “top-hat” (Carlson et al., 1982) toroidal electrostatic analyzer (EA) and a fast detection system, based on MCP electron multipliers. The ions moving along different directions in the plane of the instrument entrance aperture (different polar angle in the

---

### HIA in-flight calibration

A. Blagau et al.

---

Title Page

Abstract

Introduction

Conclusions

References

Tables

Figures

◀

▶

◀

▶

Back

Close

Full Screen / Esc

Printer-friendly Version

Interactive Discussion



## HIA in-flight calibration

A. Blagau et al.

Title Page

Abstract

Introduction

Conclusions

References

Tables

Figures

◀

▶

◀

▶

Back

Close

Full Screen / Esc

Printer-friendly Version

Interactive Discussion



upper part of Fig. 1) are deflected and focused by the EA (middle part) on the exit plane, where are recorded by a system of position encoding discrete anodes (lower part). Ion energies from 5 eV to 32 keV are sequentially measured by rapidly varying (sweeping), in logarithmically spaced steps, the voltage across the hemispherical EA plates. In the detection plane, the MCP plates are arranged in chevron pair configuration in order to achieve higher gain of secondary electrons emission. For a better detection efficiency, the ions are post-accelerated by a  $\sim 2300 - 2500$  V potential applied between the front of the MCP and a high-transparency grid located  $\sim 1$  mm above. The MCP gain can be checked by occasionally stepping this high voltage and by adjusting the discrimination level of the collecting charge amplifiers. Coverage in azimuthal angle is achieved by using the satellite spin.

To accommodate the large dynamic range of ion fluxes that occur in different regions sampled by Cluster, the entrance aperture consists of two narrow fans covering each  $180^\circ$  in polar angle and having sensitivities that differ by a factor of  $\sim 25$ . The high sensitivity (HS or “high  $G$ ”) section (entrance aperture on the right in the upper part of Fig. 1), selects ions with the appropriate energy per charge ( $E/Q$ ) and concentrates them on 16 anodes,  $11.25^\circ$  each, located in the exit plane (on the left in the bottom part of the figure). This section is designed for analyzing magnetospheric ions. Similarly, the low sensitivity (LS or “low  $g$ ”) section (entrance aperture on the left in the upper part of Fig. 1) is tuned for the detection of solar wind ions, i.e. for high ion fluxes with narrow energy and angular range. The required high angular resolution is achieved through the use of  $8 \times 5.625^\circ$  central anodes in the exit plane, the remaining 8 sectors having in principle  $11.25^\circ$  resolution. In the solar wind mode, the HIA voltage sweep is truncated when the “high  $G$ ” section is facing the Sun, in order to avoid the solar wind detection and to protect the MCP lifetime. The two sections of the instrument can supply data simultaneously in the solar wind mode.

The HIA and CODIF sensors complement each other in terms of sensitivity, mass resolution, and detection efficiency. For CODIF, an additional time-of-flight (TOF) section is present, following the  $E/Q$  selection by the EA, allowing thus the separation

of ion species. On the other hand, for the HIA detector the efficiency is much larger, primarily because this sensor has no TOF section. In addition, HIA provides a higher angular resolution (up to  $5.6^\circ \times 5.6^\circ$ , to be compared with  $11.25^\circ \times 22.5^\circ$  for CODIF) and faster electronics, capable to handle higher count rates. This makes HIA more suitable for the study of the solar wind environment. Table 1 summarizes the HIA specific parameters.

### 3 HIA operation mode and data caveats

There are 16 operating modes for the CIS instrument, that can be roughly grouped in 2 classes, i.e. “magnetospheric” and “solar wind” modes. In the “magnetospheric” modes the full energy-angle ranges are covered and the different data products are based on the counts accumulated on the “high  $G$ ” section. In the “solar wind” modes the plasma moments are based on data accumulated on the “low  $g$ ” section when this side is facing the solar wind direction. In each mode, HIA and CODIF share the telemetry bit-rate allocated to CIS for transmitting scientific products (on-board computed moments, one-, two- and three-dimensional distributions and pitch-angle distributions) to the ground.

The HIA instrument involves extensive on-board data processing, including the computation of the moments of the velocity distribution functions (density, bulk velocity vector, pressure tensor, and heat flux vector). The moments are transmitted to the ground every spin period, i.e. about 4 s. The computation uses a table of efficiency coefficients (values dependent on the energy and angular sector  $\theta$ ) based on the ground calibration performed before launch. Assuming the same energy dependence and symmetric anode efficiency evolution in time, the values of these moments are periodically adjusted on ground through the so called absolute calibration (see Sect. 4).

The transmission to the ground of the complete 3-D distribution function (i.e. at full angular and energy resolution) is not possible due to the limited telemetry rates allocated to the CIS experiment. For example, the nominal operation of HIA HS section

## HIA in-flight calibration

A. Blagau et al.

Title Page

Abstract

Introduction

Conclusions

References

Tables

Figures

⏪

⏩

◀

▶

Back

Close

Full Screen / Esc

Printer-friendly Version

Interactive Discussion



## HIA in-flight calibration

A. Blagau et al.

Title Page

Abstract

Introduction

Conclusions

References

Tables

Figures

◀

▶

◀

▶

Back

Close

Full Screen / Esc

Printer-friendly Version

Interactive Discussion



would require the transmission, every 4 s, of a matrix having 62 (or 31) energy channels  $\times$  16 elevation angles  $\times$  32 azimuth angle = 31.744 (or 15.872) elements. Therefore a reduced distribution function (particle counts typically binned in 31 energy channels and 88 angular directions) is computed on-board and transmitted to the ground with a time resolution of multiple spin periods. Based on the reduced distribution function, the so called “ground” plasma moments can be computed, where in principle correction for the efficiency energy dependence and asymmetric anode efficiency evolution can be made.

Since in the solar wind spectrogram, the  $\text{He}^{++}$  trace is clearly separated, appearing as an ion beam at roughly twice the mean proton energy, HIA is providing the plasma moments for this ion species as well. So far this data product has not been calibrated.

There are a number of data caveats of particular importance for the instrument calibration as well as for regular exploitation of HIA data. These aspects, briefly summarized below, are closely checked when selecting the calibration intervals. For a detailed discussion the reader is referred to the instrument web-page <http://cluster.irap.omp.eu/> (see also Rème et al., 2001; Dandouras and Barthe, 2012).

- The accuracy of computed moments is affected by the instrument finite energy and angle resolution, and by its finite energy range. Also, a reliable plasma moment computation requires that enough counts (minimum 100) are accumulated over the spin period.
- Inappropriate operational mode adversely affects the data accuracy. For example, when HIA is in solar wind mode while the measurements are taken in the magnetosphere, a large portion of the ion distribution is excluded. Similarly, when HIA is in the magnetospheric mode but measures in the solar wind, detector saturation may occur, leading to underestimated values for the plasma density.
- Due to the penetrating particles from the radiation belts, HIA measures a high background around perigee passes. Similar effect may occur also during some intense solar particle events.

## HIA in-flight calibration

A. Blagau et al.

Title Page

Abstract

Introduction

Conclusions

References

Tables

Figures

◀

▶

◀

▶

Back

Close

Full Screen / Esc

Printer-friendly Version

Interactive Discussion



- The detection of low-energy ions may be affected by the spacecraft charging to a positive floating potential that repels these ions.
- On some occasions, instrument artifacts (wrong time-tagging, sudden density drops, high-voltage discharges, wrong discriminator levels etc) may occur. These events are listed on the CIS Data Caveats list, available on the instrument web-page.

Since the beginning of the mission, the HIA sensors were operational only on Cluster 1 (C1) and C3. Since November 2009, after almost 10 yr of very good performance, the CIS experiment onboard C3 is not operational any more. Also, after June 2011 the HIA operations on C1 are restricted to magnetospheric modes only, with the instrument switched into a safe stand-by mode when in the solar wind.

### 4 The HIA in-flight calibration

The HIA detection efficiency as a function of position (polar angle  $\theta$ ) and particle energy  $E$  is given by the formula (see Bosqued, 2000, reporting on the HIA ground calibration)

$$\text{Eff}(\theta, E)^{-1} = \text{Norm}_\theta \cdot \text{Cheff}(\theta) \cdot \frac{A \cdot E + B}{T_0 + T_1 \cdot E_t + T_2 \cdot E_t^2}.$$

The first part of the RHS describes the position (anode) dependent efficiency, with  $\text{Norm}_\theta$  designating the anode normalization coefficients (one for each sensitivity side) and  $\text{Cheff}(\theta)$  the relative anode dependent efficiency coefficients. The second part of RHS describes the efficiency energy dependence, with  $A$ ,  $B$ ,  $T_{0,1,2}$  being the calibration coefficients and  $E_t = E + E_g$  the total energy (sum of the particle energy  $E$  and the MCP-grid acceleration energy  $E_g$ ) employed for describing the MCP energy-dependent efficiency. In total there are  $2 + 2 \cdot 16 + 2 \cdot 2 + 3 = 41$  (39 independent) efficiency calibration coefficients for each validity period and spacecraft. Their values are specified in the calibration files that are constantly provided as the mission progresses.

## HIA in-flight calibration

A. Blagau et al.

[Title Page](#)

[Abstract](#)

[Introduction](#)

[Conclusions](#)

[References](#)

[Tables](#)

[Figures](#)

[⏪](#)

[⏩](#)

[◀](#)

[▶](#)

[Back](#)

[Close](#)

[Full Screen / Esc](#)

[Printer-friendly Version](#)

[Interactive Discussion](#)



The efficiency coefficients of the HIA instruments have been determined on ground through extensive pre-flight calibrations at IRAP vacuum test facilities in Toulouse. Using ion beams of energies from a few tens of eV up to 30 keV, detailed studies of MCPs gain levels, MCP matching, and angular-energy resolution for each sector (each  $\theta$ ) were performed. Based on these tests, a table of efficiency coefficients is stored on-board in the non-volatile memory and used by the processing software to compute the on-board moments from the full angular and energy resolution 3-D ion distribution function.

However, the detector efficiencies change with time due to various reasons presented in Sect. 1. Therefore, as the missions progresses, the on-board calculation are based on out-of-date/in-accurate efficiencies. These unavoidable change with time of the channel-plate detectors require continuous in-flight calibration. Also, the MCP high voltage is periodically increased by ground commands, to compensate for the MCP gain fatigue. Since the procedure has a direct impact on detector efficiency, an in-flight calibration is subsequently required. So far, this operation has been performed five times (see Fig. 8).

The standard procedure to calibrate in-flight the HIA instrument, called the *absolute calibration*, relies on comparing HIA ion number density with the electron number density provided by the WHISPER experiment onboard Cluster (Décréau et al., 2001). While HIA detects individual particles to measure the ion distribution function, WHISPER is based on a different method to determine the plasma density, i.e. by analyzing, both actively and passively, the electric signals in the neighboring plasma. In active mode, WHISPER measures the total electron density, while in passive mode it provides a survey of natural emissions from about 2 to 80 kHz, that covers the electron plasma resonance frequency.

There are a number of assumptions involved in the absolute calibration procedure, as follows:

## HIA in-flight calibration

A. Blagau et al.

[Title Page](#)

[Abstract](#)

[Introduction](#)

[Conclusions](#)

[References](#)

[Tables](#)

[Figures](#)

[⏪](#)

[⏩](#)

[◀](#)

[▶](#)

[Back](#)

[Close](#)

[Full Screen / Esc](#)

[Printer-friendly Version](#)

[Interactive Discussion](#)



- there is a symmetric anode-dependent efficiency evolution with time, and therefore the relative anode-dependent efficiency coefficients  $C_{\text{eff}}(\theta)$ , determined in the pre-flight tests, have not changed.
- the coefficients  $A$ ,  $B$ ,  $T_{0,1,2}$ , describing the efficiency energy dependence do not change as well and assume the values determined in the pre-flight tests.
- the WHISPER data are well calibrated and free of errors (at least in the statistical sense). The traces in the WHISPER spectrograms are correctly assigned to some characteristic frequencies in plasma, from where electron density can be inferred. In these circumstances, the WHISPER data can be taken as reference.

The first two assumptions greatly simplify the calibration task, basically implying that only two coefficients (one for each sensitivity side) are needed to correct the HIA efficiency. It also means that the on-board moments are accurate up to a multiplication factor determined through calibration, allowing thus to take advantage of the HIA highest temporal, directional and energy resolution. Indeed, e.g. in magnetospheric modes the on-board moments are computed every spin period based on uncompressed data accumulated in 32 energy channels and 16 elevation  $\times$  32 azimuth solid angles (Di Lelis and Formisano, 2000), whereas the ground-computed moments are based on the reduced distribution function transmitted to the ground, having typically 31 energy  $\times$  88 solid angle bins and poorer time resolution.

Figure 2, based on C1 data from 17 October 2007, presents the individual anode response of HIA high sensitivity section in the plasma sheet environment, where the plasma distribution function is expected to be highly isotropic. Each of the panels corresponds to one sector in elevation angle ( $\theta$  angle) for the arriving particles. The relatively homogeneous response from all 8 angular sectors supports qualitatively the assumption of symmetric anode-dependent efficiency evolution with time. The same situation is observed for HIA instrument on C3 as well. Note that there are only 8 panels, although according to bottom part of Fig. 1 there should be 16 angular sectors for the HS side of HIA. This is because the distribution function sent to the ground has been re-

duced by the on-board processing software in order to comply with the limited capacity of the telemetry; in that process the counts registered by individual anodes are binned in 8 angular sectors.

Regarding the second assumption, i.e. constancy of the coefficients describing the efficiency energy dependence, there are some indications that this might not be completely valid (see e.g. the discussion about the HIA measurements in the plasma sheet environment in Sect. 6) but so far no careful study addressing this problem has been carried out. However, it seems that a change in the efficiency energy dependence is a second order effect, at least in the plasma environments where the two HIA sides are calibrated (see the statistical studies presented in Sect. 5).

One particular aspect that might be of concern is the role of ion composition in the HIA–WHISPER data comparison. The prevalent minor ions in solar wind and magnetosheath plasma (the environments where the two HIA sides are calibrated; see next sections) are the  $\alpha$  particles. If one considers a mixture of protons (number density  $N_p$ , mass  $m_p$ , and electric charge  $q_p$ ) and  $\alpha$  particles (with corresponding parameters  $N_\alpha$ ,  $m_\alpha$ , and  $q_\alpha$ ), then for a detector like HIA, unable to discriminate between the ion species, the number density reported by the instrument will be (see e.g. Paschmann et al., 1998):  $N_{\text{HIA}} = N_p + \sqrt{m_p/m_\alpha} N_\alpha = N_p + N_\alpha/2$ . On the other hand, the WHISPER instrument will report a number density  $N_{\text{WHI}} = N_p + (q_\alpha/q_p) N_\alpha = N_p + 2 N_\alpha$ . Typically, the  $\alpha$  particles abundance in the solar wind and magnetosheath plasma is around few percents of the proton number density. Therefore the discrepancy between the readings of the two instruments is of the same magnitude and consequently can be neglected in the first approximation. In addition, the procedure used to select the final set of calibration intervals (see Sect. 4.1) tends to exclude intervals with lower (than expected) value of  $N_{\text{HIA}}/N_{\text{WHI}}$  ratio.

In the case of HIA operating in “solar wind” mode, where the protons and  $\alpha$  particles are clearly separated in the energy/charge channels, the on-board software automatically computes the plasma moments separately for the two ion species. Therefore here one compares  $N_{\text{HIA}} = N_p$  with  $N_{\text{WHI}} = N_p + 2 N_\alpha$ . However, the clear separation of the

## HIA in-flight calibration

A. Blagau et al.

Title Page

Abstract

Introduction

Conclusions

References

Tables

Figures

◀

▶

◀

▶

Back

Close

Full Screen / Esc

Printer-friendly Version

Interactive Discussion



He<sup>++</sup> trace in the energy spectrogram allows us to select from the beginning intervals with low presence of  $\alpha$ , as will be described in Sect. 4.2.

#### 4.1 Calibration of HIA high sensitivity section

For calibrating the HIA high sensitivity section, magnetosheath (MS) intervals are used since the characteristic values of the plasma parameters in that environment (like density, temperature, energy spectrum within the energy domain covered by HIA) allow for an optimum instrument performance.

Each part of the year when Cluster samples the MS environment, i.e. roughly between November and June the following year, is analyzed to obtain one set of calibration coefficients. The number of values in the set depends on the efficiency evolution. Typically two values, each obtained by combining data from several intervals, are inferred. Nevertheless, when an increase in the MCP HV is commanded from ground, a sudden increase followed by a relatively rapid adjustment in efficiency is expected, which requires the determination of additional values. The last value in the set is assumed to be valid until the beginning of the next MS season.

Intervals for calibration are carefully selected to meet several criteria listed below:

- the HIA energy spectrogram suggests that, presumably, the vast majority of ions are detected, i.e. no indication of a significant ion population below or above the detector energy range exists.
- the evolution of HIA density is regular, useful for revealing potential instrument artifacts. This condition is also important because HIA and WHISPER could provide different values when a steep boundary is encountered (due to Larmor radius effects). It is desirable as well to select intervals where the density values span over a wide range, for a better comparison.
- preferably the same intervals for both C1 and C3 are used, to allow for an inter-spacecraft calibration and to detect potential instrument artifacts.

### HIA in-flight calibration

A. Blagau et al.

Title Page

Abstract

Introduction

Conclusions

References

Tables

Figures

⏪

⏩

◀

▶

Back

Close

Full Screen / Esc

Printer-friendly Version

Interactive Discussion



- intervals are not on the Data Caveat list (see Sect. 3).

For the selected intervals, the WHISPER density data are requested from the instrument team, that either decides to re-generate it for the purpose of HIA calibration or to re-validate the already available CAA data set.

Figure 3 illustrates one example of interval selected for HIA–WHISPER density comparison. The four panels at the top represent the type of plot routinely produced for the identification of calibration intervals. First, the HIA energy spectrograms in three ranges, i.e. above 2 keV, the entire energy range, and below 100 eV, are shown in order to identify intervals that better comply with the requirement that virtually all particles are detected by the instrument. In the fourth panel the HIA (red) and WHISPER (black) raw density data are shown. Here a few sudden HIA density drops can be seen; these signatures are not present in the WHISPER data and are interpreted as instrument artifacts. The next panel compares the two densities after the data processing has been performed, which includes instrument artifacts removal, discarding of short intervals with rapid variation in density, data filtering, averaging and interpolation etc. The sixth panel checks the plasma gyrotropy as measured by the quantity  $(\rho_{\perp 2} - \rho_{\perp 1})/[(\rho_{\perp 2} + \rho_{\perp 1})/2]$ , with  $\rho_{\perp 1}$  and  $\rho_{\perp 2}$  being the plasma thermal pressure along two orthogonal directions in the plane perpendicular to the magnetic field. The relatively small deviations from gyrotropy, e.g. around or below 5%, provides supporting evidence of HIA symmetric anode response for this interval. The bottom panel shows the  $N_{\text{HIA}}/N_{\text{WHI}}$  density ratio (blue) and its average value for this interval (magenta straight line).

The result of comparison can also be shown in the form of HIA vs. WHISPER density plot, presented in Fig. 4, where the left part refers to the event described above. The points are clearly scattered along the regression line (in red) forced to cross the origin; its slope is used to estimate of the calibration factor inferred from this interval. The average value of several calibration factors, obtained from different intervals, is then employed to update the calibration files used in processing the HIA data.

## HIA in-flight calibration

A. Blagau et al.

[Title Page](#)

[Abstract](#)

[Introduction](#)

[Conclusions](#)

[References](#)

[Tables](#)

[Figures](#)

[I◀](#)

[▶I](#)

[◀](#)

[▶](#)

[Back](#)

[Close](#)

[Full Screen / Esc](#)

[Printer-friendly Version](#)

[Interactive Discussion](#)



## HIA in-flight calibration

A. Blagau et al.

Title Page

Abstract

Introduction

Conclusions

References

Tables

Figures

◀

▶

◀

▶

Back

Close

Full Screen / Esc

Printer-friendly Version

Interactive Discussion



In spite of the careful selection, it can happen that the HIA–WHISPER data comparison brings inconsistent results on some intervals. Typically a lower (than expected) value of the  $N_{\text{HIA}}/N_{\text{WHI}}$  ratio is attributed to the presence of plasma population outside the HIA detection range, to the spacecraft charging or to events with relatively high abundance of  $\alpha$  particles. Therefore, the final set of intervals to be used in the calibration is established after an additional inter-spacecraft comparison and/or checking the data provided by other instruments like CODIF, ASPOC, EFW (spacecraft potential).

### 4.2 Calibration of HIA LS section

With some specific differences, the calibration of the HIA low sensitivity section follows a similar procedure. One uses solar wind (SW) data and compares the HIA and WHISPER density on carefully selected intervals.

The selection is based on the type of plot presented in Fig. 5. The top panel shows HIA (red) and WHISPER (black) raw density data, A number of sudden HIA density drops (instrument artifacts), can be seen here as well. In the second panel the energy spectrogram based on data accumulated on the LS and is shown. For the purpose of calibration, it is desirable to select events with low presence of  $\alpha$  particles, (seen in the second panel as the faint green line, at around twice the peak proton energy). Since an accurate calibration of the LS section requires no significant counts accumulated on the HS section (blocked when facing the SW direction, see Sect. 2), the third and the fourth panel present the plasma density and the energy spectrogram based on data accumulated on this side. The bottom panel compares the LS (red) and HS (black) count rates.

After the selection of SW intervals suitable for calibration, the raw HIA and WHISPER data are processed in a manner similar to that described in the previous section. For the event presented above, the result of the comparison is showed in the right part of Fig. 4 in the form of HIA vs. WHISPER density plot. The points are aligned along the regression line (in red) forced to cross the origin; its slope is taken as the value of the calibration factor corresponding to this interval. By averaging several calibration factors,





an increase has been noticed. Note also that sometimes the efficiency has slightly increased without raising the MCP HV, like at the end of 2007. This unexpected behavior has been observed on both spacecraft and on both sensitivities, i.e. both on MS and SW intervals, which argues for a real effect. An MCP efficiency recovery has also been reported by the PEACE team in that period.

The HIA in-flight calibration is a complex task that requires considerable effort. This activity will continue and expand in order to ensure the highest data accuracy. Below we present a list of topics to be addressed in the future:

- to apply the calibration methodology described in this paper to data provided by HIA in the first years of the Cluster mission, i.e. before October 2005.
- to investigate more closely whether or not the anode-dependent efficiency factors evolved symmetrically in the course of the mission. Although Fig. 2 indicates a relatively homogeneous response from all HIA angular sectors, no quantitative assessment of this assumption was made so far and only few data intervals have been qualitatively evaluated. In the case of CODIF such an investigation is regularly performed, bringing significant improvements to data quality.
- to investigate possible changes in the efficiency energy dependence in the course of the mission.
- to calibrate the He<sup>++</sup> data provided by HIA in the SW.

Related to the third item above, there is evidence suggesting the need for correction of the efficiency energy dependence. Figure 9 shows a comparison between HIA and CODIF data in the plasmashet environment on 7 September 2001. The energy spectrograms (CODIF first panel and HIA the second panel) support the idea that most of the particles are detected by the two instruments. However, the plasma pressure and density (next panels) are different, with HIA (red lines) providing values around 2 times lower than CODIF (black lines). The two instruments are calibrated and there is convincing evidence that CODIF provides the right measurements.

**HIA in-flight calibration**

A. Blagau et al.

Title Page

Abstract

Introduction

Conclusions

References

Tables

Figures

⏪

⏩

◀

▶

Back

Close

Full Screen / Esc

Printer-friendly Version

Interactive Discussion





HIA in-flight  
calibration

A. Blagau et al.

Title Page

Abstract

Introduction

Conclusions

References

Tables

Figures

◀

▶

◀

▶

Back

Close

Full Screen / Esc

Printer-friendly Version

Interactive Discussion



- (CAA), in: *The Cluster Active Archive, Studying the Earth's Space Plasma Environment*, edited by: Laakso, H., Taylor, M., and Escoubet, C. P., Springer, Berlin, 51–72, 2010. 409
- Dandouras, I., Barthe, A., Kistler, L. M., and Blagau, A.: Calibration Report of the CIS measurements in the Cluster Active Archive (CAA), [http://caa.estec.esa.int/caa/ug\\_cr\\_icd.xml](http://caa.estec.esa.int/caa/ug_cr_icd.xml) (last access: 4 July 2013), 2012. 409
- Décrou, P. M. E., Fergeau, P., Krasnoselskikh, V., Le Guirriec, E., Lévêque, M., Martin, P., Randriamboarison, O., Rauch, J. L., Sené, F. X., Séran, H. C., Trotignon, J. G., Canu, P., Cornilleau, N., de Féraudy, H., Alleyne, H., Yearby, K., Mögensen, P. B., Gustafsson, G., André, M., Gurnett, D. C., Darrouzet, F., Lemaire, J., Harvey, C. C., Travnicek, P., and Whisper Experimenters Group: Early results from the Whisper instrument on Cluster: an overview, *Ann. Geophys.*, 19, 1241–1258, doi:10.5194/angeo-19-1241-2001, 2001. 414
- Di Lelis, A. M. and Formisano, V.: Cluster CIS-2 Instrument, FM Normal Operation Software, CNR IFSI report, Frascati, 2000. 415
- Ganushkina, N. Y., Dandouras, I., Shprits, Y. Y., and Cao, J.: Locations of boundaries of outer and inner radiation belts as observed by Cluster and Double Star, *J. Geophys. Res. Space Phys.*, 116, A09234, doi:10.1029/2010JA016376, 2011. 423
- Klumpar, D. M., Möbius, E., Kistler, L. M., Popecki, M., Hertzberg, E., Crocker, K., Granoff, M., Tang, L., Carlson, C. W., McFadden, J., Klecker, B., Eberl, F., Küneth, E., Kästle, H., Ertl, M., Peterson, W. K., Shelly, E. G., and Hovestadt, D.: The Time-of-Flight Energy, Angle, Mass Spectrograph (Teams) Experiment for Fast, *Space Sci. Rev.*, 98, 197–219, 2001. 427
- Paschmann, G., Fazakerley, A. N., and Schwartz, S. J.: Moments of plasma velocity distributions, in: *Analysis Methods for Multi-Spacecraft Data*, edited by: Paschmann, G. and Daly, P. W., ISSI Scientific Reports, ESA Publications Division, Noordwijk, 125–158, 1998. 416
- Prince, R. H. and Cross, J. A.: Gain Fatigue Mechanism in Channel Electron Multipliers, *Rev. Sci. Instrum.*, 42, 66–71, doi:10.1063/1.1684879, 1971. 408
- Rème, H., Aoustin, C., Bosqued, J. M., Dandouras, I., Lavraud, B., Sauvaud, J. A., Barthe, A., Bouyssou, J., Camus, Th., Coeur-Joly, O., Cros, A., Cuvilo, J., Ducay, F., Garbarowitz, Y., Medale, J. L., Penou, E., Perrier, H., Romefort, D., Rouzaud, J., Vallat, C., Alcaydé, D., Jacquy, C., Mazelle, C., d'Uston, C., Möbius, E., Kistler, L. M., Crocker, K., Granoff, M., Mouikis, C., Popecki, M., Vosbury, M., Klecker, B., Hovestadt, D., Kucharek, H., Kuenneth, E., Paschmann, G., Scholer, M., Sckopke, N., Seidenschwang, E., Carlson, C. W., Curtis, D. W., Ingraham, C., Lin, R. P., McFadden, J. P., Parks, G. K., Phan, T., Formisano, V., Amata, E., Bavassano-Cattaneo, M. B., Baldetti, P., Bruno, R., Chionchio, G., Di Lellis, A., Mar-

# GID

3, 407–435, 2013

## HIA in-flight calibration

A. Blagau et al.

[Title Page](#)

[Abstract](#)

[Introduction](#)

[Conclusions](#)

[References](#)

[Tables](#)

[Figures](#)

[I◀](#)

[▶I](#)

[◀](#)

[▶](#)

[Back](#)

[Close](#)

[Full Screen / Esc](#)

[Printer-friendly Version](#)

[Interactive Discussion](#)



cucci, M. F., Pallochia, G., Korth, A., Daly, P. W., Graeve, B., Rosenbauer, H., Vasyliunas, V., McCarthy, M., Wilber, M., Eliasson, L., Lundin, R., Olsen, S., Shelley, E. G., Fuselier, S., Ghielmetti, A. G., Lennartsson, W., Escoubet, C. P., Balsiger, H., Friedel, R., Cao, J.-B., Kovrazhkin, R. A., Papamastorakis, I., Pellat, R., Scudder, J., and Sonnerup, B.: First multi-spacecraft ion measurements in and near the Earth's magnetosphere with the identical Cluster ion spectrometry (CIS) experiment, *Ann. Geophys.*, 19, 1303–1354, doi:10.5194/angeo-19-1303-2001, 2001. 408, 412, 426, 427

5

Vallat, C.: Evaluation des performances en vol des détecteurs de l'expérience "Cluster Ion Spectrometry", CNRS report, Toulouse, 2001. 409

HIA in-flight  
calibration

A. Blagau et al.

[Title Page](#)[Abstract](#)[Introduction](#)[Conclusions](#)[References](#)[Tables](#)[Figures](#)[◀](#)[▶](#)[◀](#)[▶](#)[Back](#)[Close](#)[Full Screen / Esc](#)[Printer-friendly Version](#)[Interactive Discussion](#)**Table 1.** The HIA specific parameters according to Rème et al. (2001) and Dandouras and Barthe (2012).

Energy range (eV)		$\sim 5\text{--}32 \times 10^3$
Energy resolution $\Delta E/E$ (FWHM, %)		$\sim 16$
No. of $E$ microsteps		124
Time resolution (s)	2-D	$62.5 \times 10^{-3}$
	3-D	4
Angular resolution (deg)	LS	$\sim 5.6 \times 5.6$
	HS	$\sim 12.5 \times 5.6$
Geom. factor ( $\text{cm}^2 \text{sr keV/keV}$ )	LS	$1.9 \times 10^{-4}$
	HS	$4.9 \times 10^{-3}$
Dynamic range ( $\text{cm}^2 \text{s sr}^{-1}$ )	LS	$10^6 - 2 \times 10^{10}$
	HS	$10^4 - 2 \times 10^8$
Lower limit density value ( $\text{cm}^{-3}$ )		$0.01 \div 0.02$

## HIA in-flight calibration

A. Blagau et al.

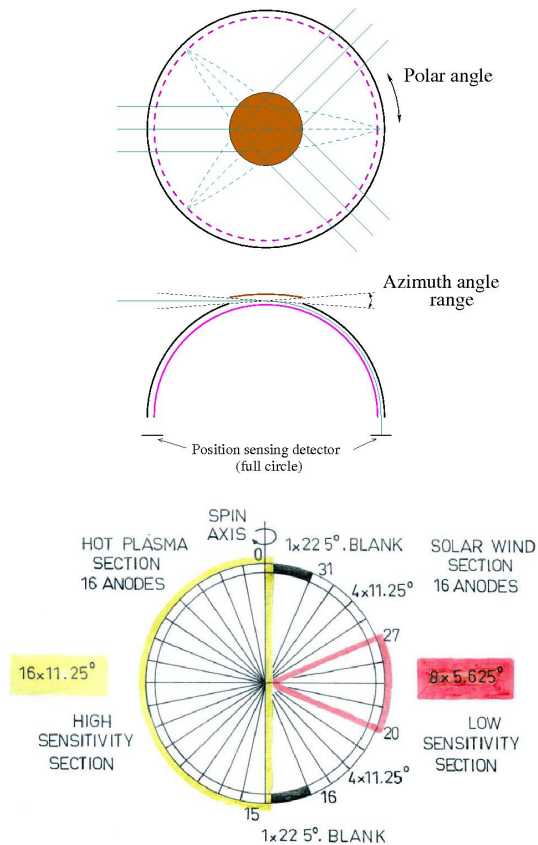


**Fig. 1.** The first two parts present the top view and cross-sectional view of the HIA instrument. At the bottom, the principles of HIA anode sectoring are shown. In the upper and bottom parts of the figure, the spin axis is in the plane of the paper, along the vertical direction, while in the middle part it points into the paper. See text for more details. Figure adapted from Klumpar et al. (2001) and Rème et al. (2001).

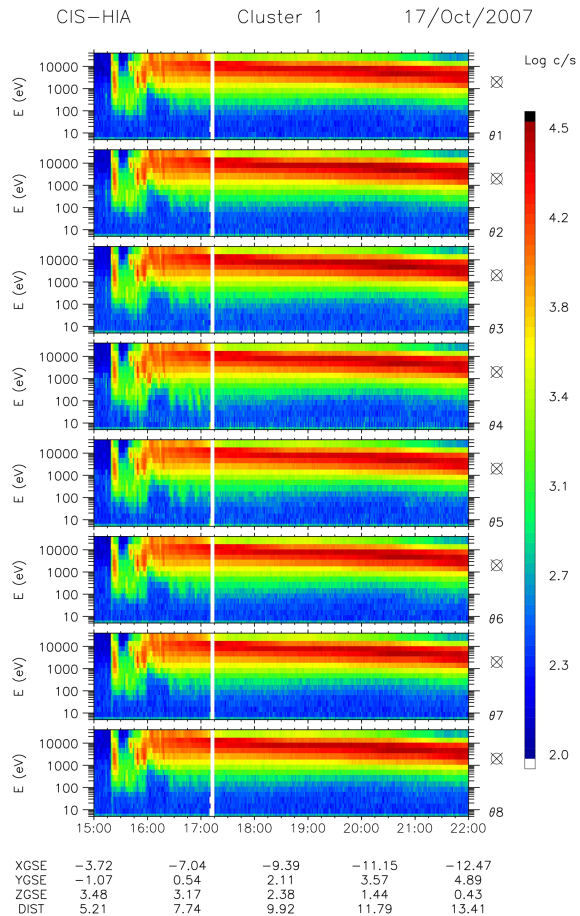


**Fig. 2.** Individual anode response of HIA high sensitivity section in the plasma sheet, an environment where plasma distribution function is highly isotropic. Only C1 data are shown. Each of the panels corresponds to one sector in elevation angle for the arriving particles.

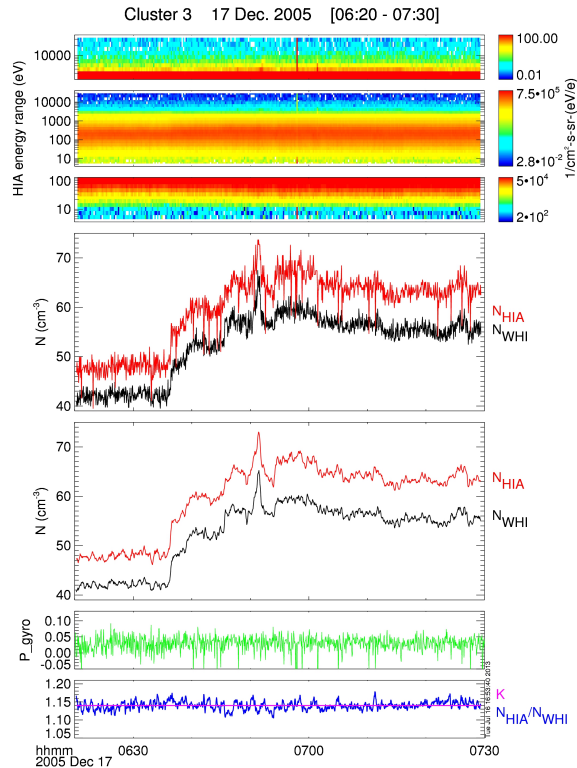


**Fig. 3.** Calibration of HIA HS section. The top panels show ion energy spectrograms in three ranges, i.e. above 2 keV, the entire HIA energy range, and below 100 eV. The next panel presents HIA (red) and WHISPER (black) raw density data while in the fifth panel, the data from the two instruments is processed. The sixth panel presents the deviation in gyrotropy, based on the relative differences between the perpendicular pressure components. The bottom panel shows the ratio between the two densities (blue) and its average value  $K$  (magenta straight line). More explanations are provided in the text.

HIA in-flight  
calibration

A. Blagau et al.

Title Page

Abstract

Introduction

Conclusions

References

Tables

Figures

◀

▶

◀

▶

Back

Close

Full Screen / Esc

Printer-friendly Version

Interactive Discussion

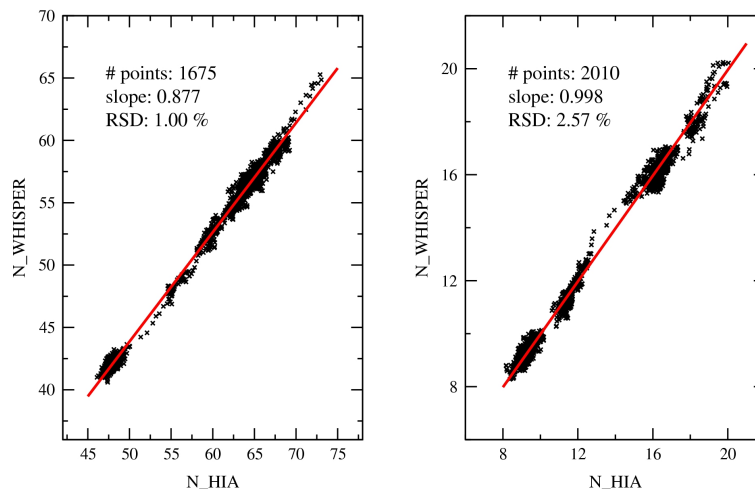


**Fig. 4.** HIA vs. WHISPER density comparison for the events presented in Fig. 3 (left panel) and in Fig. 5 (right panel), employed to calibrate the HIA HS and LS sections, respectively. The slope of the regression line crossing the origin (in red) is used to estimate the calibration factor for the corresponding interval.

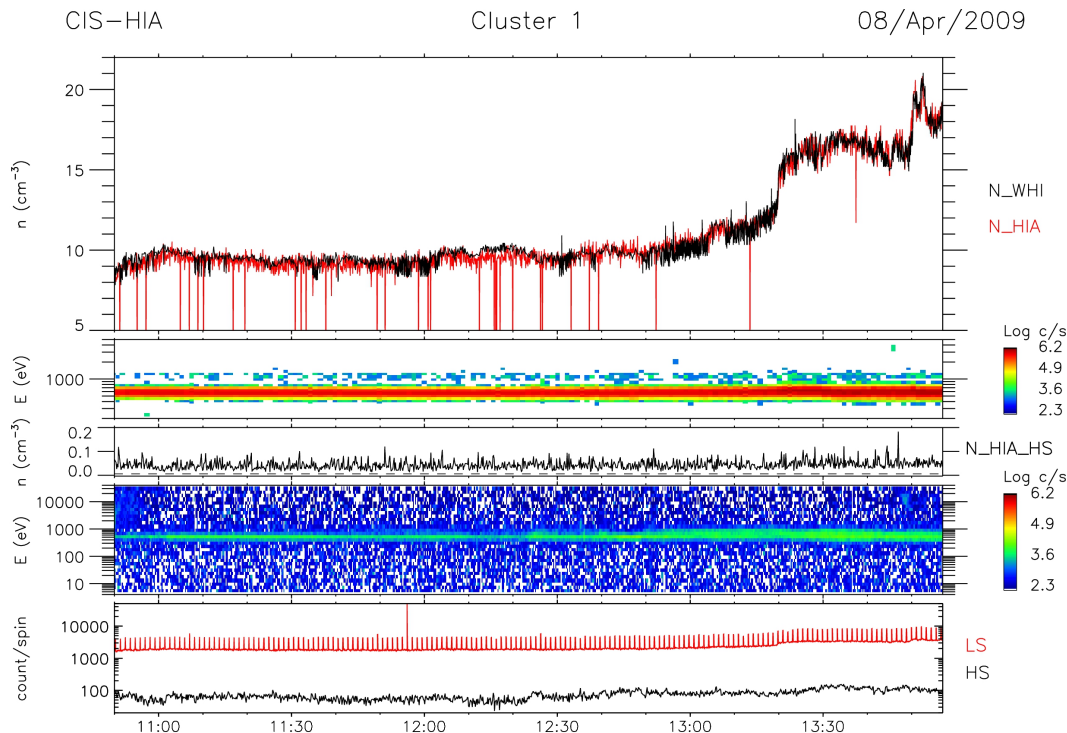


**Fig. 5.** Standard plot used for identification of suitable HIA LS calibration intervals. From top to bottom, the individual panels present: HIA (red) and WHISPER (black) raw density data, the energy spectrogram provided by the LS section, the number density based on data collected by the HS section, the energy spectrogram provided by the HS section, and the number of counts detected by LS (red) and HS (black) sections.

[Title Page](#)
[Abstract](#)
[Introduction](#)
[Conclusions](#)
[References](#)
[Tables](#)
[Figures](#)
[⏪](#)
[⏩](#)
[⏴](#)
[⏵](#)
[Back](#)
[Close](#)
[Full Screen / Esc](#)
[Printer-friendly Version](#)
[Interactive Discussion](#)


## HIA in-flight calibration

A. Blagau et al.

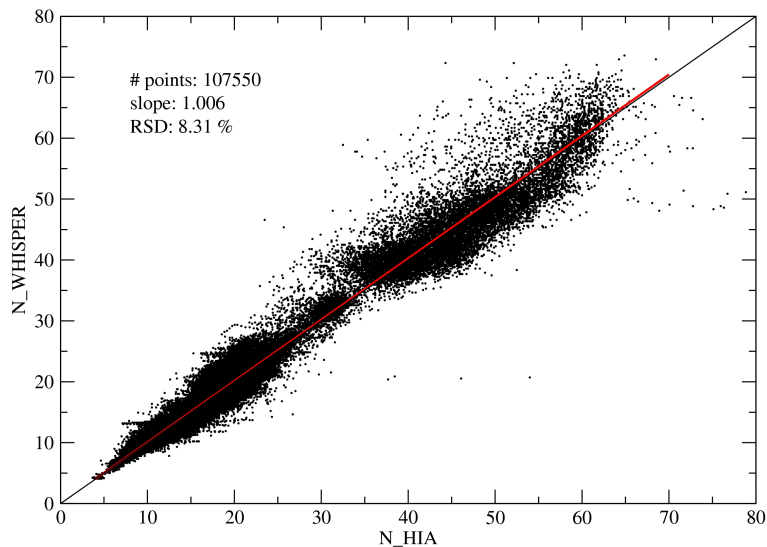


**Fig. 6.** Comparison between calibrated HIA and WHISPER data on Cluster 1. All magnetosheath intervals sampled by HIA HS side between 15 December 2006 and 15 February 2007 were selected for comparison using selection criteria similar to those presented in Sect. 4. The regression line crossing the origin is shown in red.

[Title Page](#)[Abstract](#)[Introduction](#)[Conclusions](#)[References](#)[Tables](#)[Figures](#)[◀](#)[▶](#)[◀](#)[▶](#)[Back](#)[Close](#)[Full Screen / Esc](#)[Printer-friendly Version](#)[Interactive Discussion](#)

**HIA in-flight calibration**

A. Blagau et al.

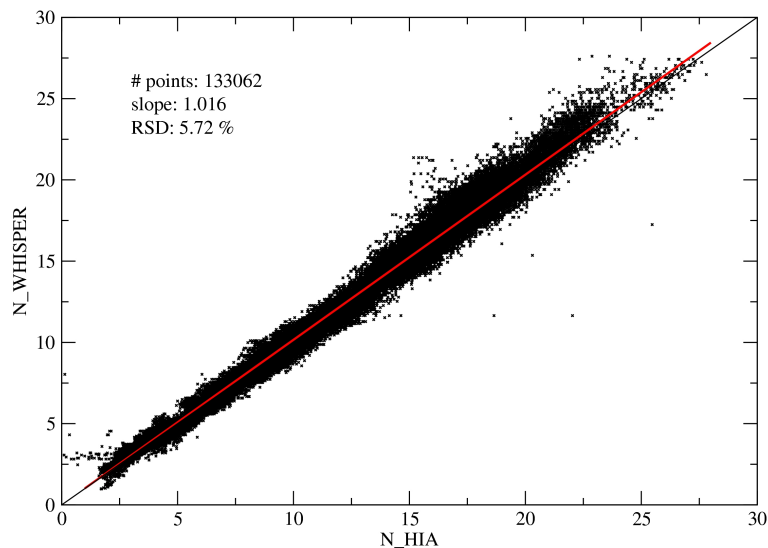


**Fig. 7.** Comparison between calibrated HIA and WHISPER data on Cluster 1. All solar wind intervals sampled by HIA LS side between 15 December 2006 and 15 February 2007 were selected for comparison using selection criteria similar to those presented in Sect. 4. The regression line crossing the origin is shown in red.

[Title Page](#)[Abstract](#)[Introduction](#)[Conclusions](#)[References](#)[Tables](#)[Figures](#)[◀](#)[▶](#)[◀](#)[▶](#)[Back](#)[Close](#)[Full Screen / Esc](#)[Printer-friendly Version](#)[Interactive Discussion](#)

## HIA in-flight calibration

A. Blagau et al.

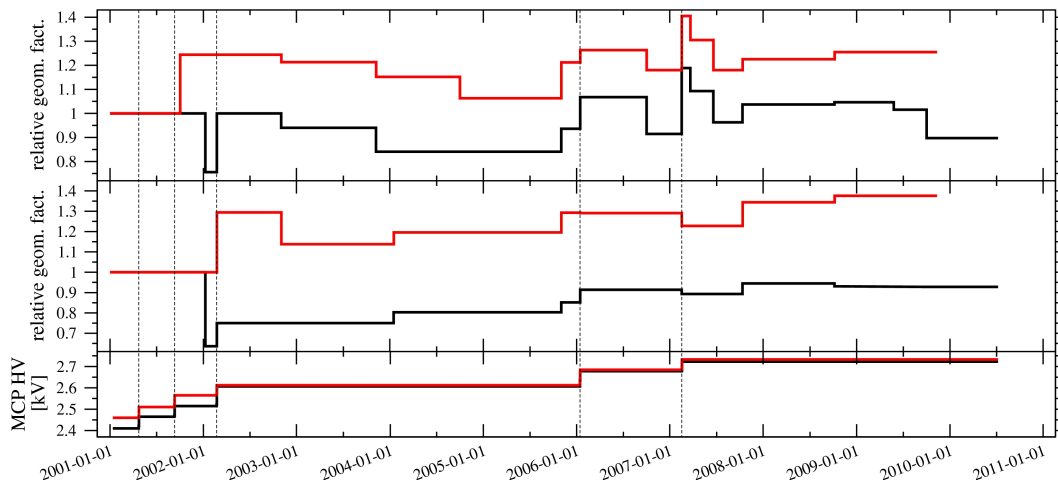


**Fig. 8.** Evolution of the HIA HS and LS efficiency (top and middle panel, respectively), and of the high voltage applied to the MCPs (bottom panel). Black lines refer to C1 and red lines to C3. The time axis spans from 1 January 2001 (around the start of Cluster operational phase) to the beginning of 2011. The dates of MCP HV increase are also shown by vertical dashed lines.

Title Page

Abstract

Introduction

Conclusions

References

Tables

Figures

◀

▶

◀

▶

Back

Close

Full Screen / Esc

Printer-friendly Version

Interactive Discussion



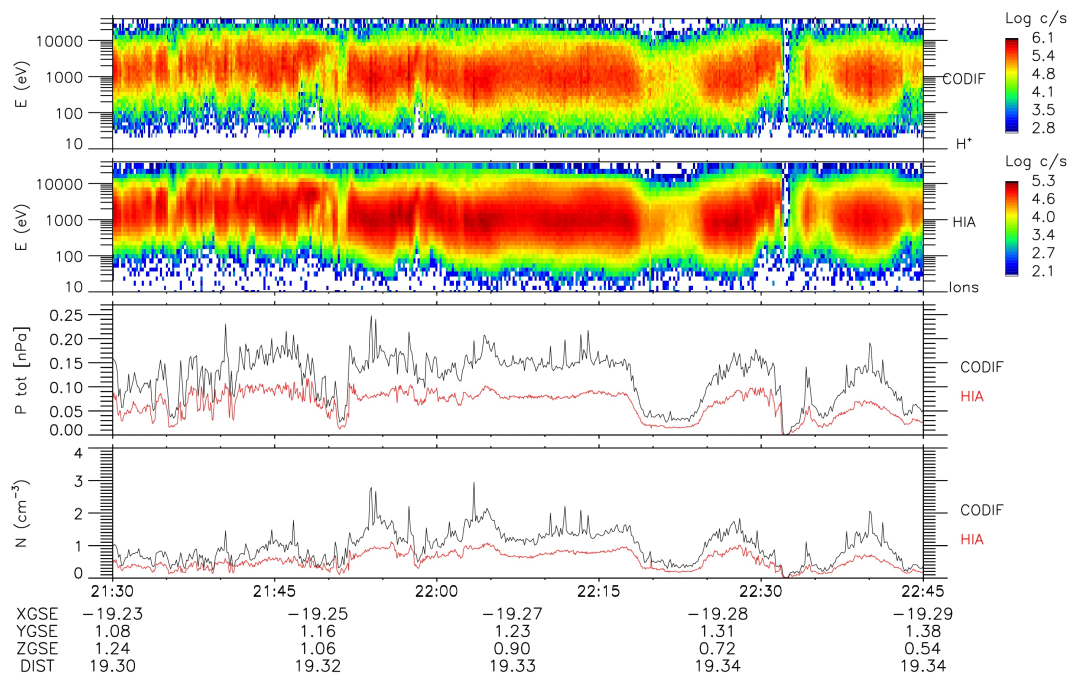


**Fig. 9.** CODIF and HIA data comparison in the plasma sheet region. From top to bottom, the first two panels show the differential energy spectrogram from CODIF and HIA, respectively. The next two panels show the plasma pressure and plasma density as provided by CODIF (black line) and HIA (red line).

**HIA in-flight calibration**

A. Blagau et al.

Title Page

Abstract

Introduction

Conclusions

References

Tables

Figures

◀

▶

◀

▶

Back

Close

Full Screen / Esc

Printer-friendly Version

Interactive Discussion

